Revealing the trehalose mediated inhibition of protein aggregation through lysozyme–silver nanoparticle interaction†

Soumik Siddhanta,‡[a] Ishan Barman*[bc] and Chandrabhas Narayana*[a]

We propose a facile and robust carbohydrate-mediated method for the prevention of nanoparticle induced denaturation and aggregation of proteins. Using label-free plasmon-enhanced Raman spectroscopy measurements, the mechanistic principles of trehalose stabilization in a model protein–nanoparticle system are elucidated for the first time, facilitating its further application in diagnostic and therapeutic nanoplex development.

Introduction

Nanoparticles offer an intriguing platform in biomedicine – possessing singular mechanical, optical and plasmonic properties yet constrained by toxicity considerations. On one hand, they can be harnessed for a wide gamut of applications ranging from targeted drug delivery[1] and therapeutics[2] to ultrasensitive biodetection,[3] but on the other hand, they represent cytotoxic contaminants[4] which can adversely affect a biosystem in diverse (and potentially unknown) ways.[5] One of the most important components of any biosystem is proteins. Folded into unique three-dimensional conformations, they are responsible for essential functions in an organism. In addition to their ubiquitous presence in biological tissue, proteins are key to the formulation of peptide based therapeutics.[6] Thus maintaining the structure and active state of protein, and prevention of aggregation are the main determinants of maintaining potency, stability and shelf-life. Specifically, the inability to maintain the former has been reported during protein–nanoparticle interactions, where the protein undergoes conformational change(s) and loses its function.[7] The mechanism of interaction between protein and the nanoparticle surface is a matter of ongoing debate but this outcome has been a major impediment in the preparation of stable protein–nanoparticle complexes tailored for theranostics. Moreover, protein aggregation due to nanoparticle conjugation can be toxic as it may increase the immunogenicity and lead to undesired side effects.[8]

One of the most common strategies adopted to prevent protein denaturation is to coat nanoparticles with a biocompatible material, which stabilizes the protein or shields the protein from coming in direct contact with the nanoparticle surface.[7] This approach, however, proves to be counter-productive for biospecies detection as optical tools, such as surface plasmon resonance and surface enhanced Raman spectroscopy (SERS), necessitate direct contact between the metal surface and protein residues for ultrasensitive transduction of molecular information. Therefore, superior strategies are urgently required to prevent the loss of protein structure and function in close vicinity of nanoparticle surfaces. Such preservation techniques can have direct implications for multi-target therapeutics[9] where proteins and nanoparticles can be used in conjunction to combat multigenic diseases as well as for targeted theranostic nanoplexes to enable cancer-selective therapy.

Osmolytes, notably sugars, have been found to provide excellent stability to proteins when subjected to chemical and thermal stress or dehydrated conditions.[10] They mimic the activity of molecular chaperones or heat shock proteins, which facilitates the folding of protein from disordered polypeptide to the native state and also prevents it from misfolding and aggregation.[11] Consequently, cells accumulate specific osmolytes for maintaining protein folding processes and modulating protein–protein interactions. We conjectured that the principles of this carbohydrate action could be significantly extended to address the aforementioned concerns of protein–nanoparticle interactions.

In this milieu, we seek to specifically explore the potential of trehalose, a non-reducing disaccharide, that provides exceptional stability to proteins from thermal stresses and is used in freeze drying of proteins to conserve their structures.[12] Being chemically

[a] Light Scattering Laboratory, Chemistry & Physics of Materials Unit, Jawaharlal Nehru Centre for Advanced Scientific Research, Jakkur P.O., Bangalore 560 064, India. E-mail: cbhas@jncasr.ac.in

[b] Department of Mechanical Engineering, Johns Hopkins University, Baltimore, Maryland 21218, USA. E-mail: ibarman@jhu.edu

[c] Department of Oncology, Johns Hopkins University School of Medicine, Baltimore, Maryland 21287, USA

† Electronic supplementary information (ESI) available. See DOI: 10.1039/c5sm01896j

‡ Present address: Department of Mechanical Engineering, Johns Hopkins University, Baltimore, Maryland 21218, USA.

inert, there are different mechanisms proposed for the protein stabilizing effect of trehalose. Broadly, three main hypotheses have been put forth to explain the singular stabilization behaviour of trehalose.[13] The first hypothesis refers to mechanical entrapment or vitrification, where the trehalose molecules form a glassy matrix entrapping the protein molecules. Thus, the native structure is protected in high concentrations of trehalose. Second, the water replacement conjecture suggests that the protein is stabilized by hydrogen bonding with the trehalose molecule thus preventing their destabilization. Finally, the water entrapment hypothesis proposes that the water molecules are trapped between the sugar molecules and the surface of the protein. In practice, the vitrification theory is observed to hold good mostly for dry or very high trehalose containing (>1 M) systems.[14] In contrast, the water replacement and entrapment theories are more prevalent in aqueous solutions of lower concentrations.[15]

Here we have employed this exceptional protein stabilizing effect of trehalose on a model protein lysozyme, which is known to denature upon interaction with noble metal nanoparticles.[16] Lysozyme forms well-characterized aggregates on the surface of metallic nanoparticles, which induces misfolding of proteins and catalyzes aggregate formation.[16] In this study, we have investigated the role of trehalose in the interaction of lysozyme with silver nanoparticles through SERS measurements. The aggregation behaviour has been studied using UV-visible absorption spectroscopy, while the changes in secondary structures have been monitored by circular dichroism (CD). Through these careful analytical measurements, we demonstrate the utility of the trehalose environment in maintaining intact protein structures, which otherwise undergo structural denaturation upon nanoparticle induced stress.

Experimental

Materials

Lyophilized chicken egg white lysozyme (molecular weight, M_W, 14.7 kDa), trehalose dihydrate, silver nitrate and sodium citrate were obtained from Sigma Aldrich and used without further purification. Potassium hydrogen phosphate and potassium dihydrogen phosphate (sigma) were used to prepare buffer solutions using ultrapure Milli Q water.

Preparation of silver nanoparticles

Colloidal silver nanoparticles were synthesized by following the standard Lee–Meisel method using sodium citrate as a reducing as well as capping agent.[17] The nanoparticles were characterized by transmission electron microscopy and UV-visible spectroscopy. The concentration of silver nanoparticles was calculated by the Beer–Lambert law using epsilon values reported in the literature.[18]

Circular dichroism studies

The effect of nanoparticles on the lysozyme structure in liquid solutions was studied by circular dichroism (CD). The concentration

of protein was maintained at around 10 μM in 10 mM potassium phosphate buffer (pH 7.4) using a JASCO spectrometer. A quartz cuvette of 1 mm path-length was used to acquire the CD spectrum. Each dataset was an average of three scans between 200 nm to 290 nm. The buffer spectrum was subtracted to obtain the final spectrum (molar residual ellipticity vs. wavelength) for analysis of secondary structures.

Fluorescence quenching studies

Fluorescence quenching of the tryptophan residues upon interaction with silver nanoparticles at various concentrations of trehalose (0, 0.05 M and 0.5 M) was studied by excitation at 290 nm and emission in the range of 300–400 nm. The concentration of protein was maintained at 1 μM in 10 mM potassium phosphate buffer and the amount of silver nanoparticle quencher was varied to obtain the fluorescence spectra.

UV-vis absorbance studies

The UV-vis absorbance studies on nanoparticle aggregation were performed in the presence of different concentrations of trehalose (0 M, 0.05 M and 0.5 M) as a function of time. The concentration of protein was kept at 1 nM and the initial optical density of the nanoparticle solution was adjusted to 1. The absorbance was measured for the solution at the interval of every 5 minutes. The UV-vis studies were also conducted in the presence of 1 M sucrose.

Confocal fluorescence microscopy

For confocal fluorescence imaging, an LSM 510 META scanning confocal microscope with a Plan Apochromat 63× oil-immersion lens (NA = 1.4) (Zeiss, Germany) was used. The microscope was controlled using Zeiss LSM acquisition software. The nanoparticle aggregates were prepared by incubating silver nanoparticle solution with lysozyme/trehalose for 30 minutes. The solution was drop casted onto a quartz coverslip and attached to a glass slide for imaging in an inverted geometry. An argon laser with an excitation wavelength of 488 nm was used for imaging.

Surface enhanced Raman spectroscopy (SERS)

The SERS spectra of lysozyme (1 μM) were collected at different trehalose concentrations (0, 0.05 and 0.5 M respectively) in Ag nanoparticle solution by using water immersion 60× infinity-corrected objective (Nikon Plan Apo, Japan, NA 0.9). 180° back-scattering geometry was used to record the SERS spectra. The excitation source was 532 nm from a diode pumped frequency doubled Nd:YAG solid state laser (Photop Suwtech Inc., GDLM-5015 L). A custom built Raman spectrometer equipped with an SPEX TRIAX 550 monochromator and a liquid nitrogen cooled CCD was used to record the spectra. A holographic 1800 grooves mm^{-1} grating was used along with the 200 μm spectrograph entrance slit setting, providing ≈ 3 cm^{-1} resolution. The accumulation time of the spectra was 30 s and a 5 point FFT filter was used for smoothening of the spectra.
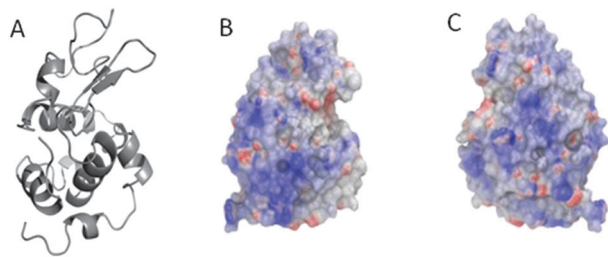
Fig. 1 (A) Schematic cartoon representation of the lysozyme protein molecule. (B) and (C) Representation of electrostatic surface charges (blue: positive, red: negative) on lysozyme molecules (rotated by 180°). Figures created using PyMOL [http://www.pymol.org] and PDB file 193L.

Results and discussion

Conjugation of protein to the nanoparticle surface

The plasmonic citrate capped silver nanoparticles used in this study are extensively used as substrates for analytical techniques, notably SERS for detection and characterization of a variety of analyte molecules.[19] Citrate being a weak capping agent can be easily replaced by the ligand molecules as well as proteins.[20] Lysozyme was chosen for the study as it is widely used as a model in experiments related to protein structure and stability.[21] It is a 14.7 kDa protein consisting of 129 amino acids whose interaction with various polyols and sugars has been well documented.[22] The isoelectric point of lysozyme is 11.35 making it positively charged at physiological pH. The positively charged domains of the lysozyme molecules (Fig. 1) are attracted to the negatively charged nanoparticle surface through electrostatic attraction. Moreover, the small size of the lysozyme molecule makes it amenable for attachment to the nanoparticle surface, which then enables greater inter-protein interactions through the side chains. It is worth noting that the protein molecules exist in a dynamic equilibrium with the surface of the nanoparticle.[23]

Specifically, it has been previously reported that lysozyme changes its conformation on the surface of metallic nanoparticles.[16] The protein molecules are partially unfolded upon adsorption onto the surface of the nanoparticles. This triggers the seeding of further protein aggregation on nanoparticle surfaces *via* protein–protein interactions and, subsequently, aggregation of the protein–nanoparticle complexes.[16] This type of protein aggregation hampers its function in physiological environments. Our efforts have been directed towards alleviating this problem and retaining the structure of the protein in the presence of nanoparticles by preventing the formation of protein–nanoparticle aggregates.

Circular dichroism studies to determine secondary structural changes

We conducted CD spectroscopic studies to determine the effect of nanoparticles on the structure of lysozyme with and without the presence of trehalose (Fig. 2). The CD spectrum of α-helical components of proteins consists of two negative peaks at 208 and 220 nm.[24] The band at 220 nm corresponds to the hydrogen-bonding environment of the secondary structure and is length independent.[24,25] The percentage of α-helicity was calculated
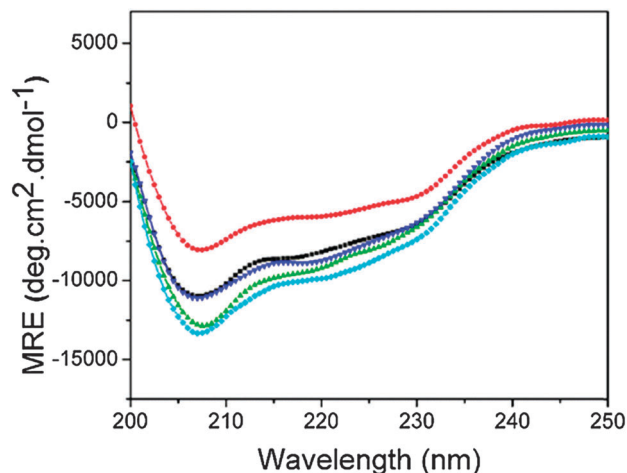

Fig. 2 Circular dichroism spectra of lysozyme in the presence of Ag nanoparticles and different concentrations of trehalose. The trehalose concentrations used are 0 M (red), 0.05 M (blue) and 0.5 M (green). The CD spectra of lysozyme in 0.5 M trehalose (without nanoparticles) and in phosphate buffer (without nanoparticles) are shown in cyan and black, respectively.

from the molar residual ellipticity (MRE) which is given by the following equation:[26]

$$\theta_{MRE} \left(\text{deg cm}^2 \text{ dmol}^{-1} \right) = \frac{\theta}{C_p n l \times 10}$$

where θ is the observed ellipticity in mdeg, C_p is the molar concentration of the protein, n is the number of residues in the protein molecule and l is the path-length of the cell.

The percentage of α-helix was calculated by the following equation:[26]

$$\alpha\text{-helix content} = \frac{[\theta_{MRE,208}] - 4000}{33\,000 - 4000}$$

The CD spectrum, which encodes information of the secondary structural components of proteins, showed a reduction of the α-helix content of lysozyme in the presence of nanoparticles (red curve) with respect to the native protein (black curve) (Fig. 2). Our observation is consistent with the reduction of the α-helix content upon interaction of a protein with a hydrophilic surface indicating a structural disorganization.[27] Our calculations reveal that lysozyme in phosphate buffer has an α-helix content of 23.45%, whereas the introduction of nanoparticles significantly reduces the same to a mere 14.55%. These α-helix content values of lysozyme are consistent with previously reported values calculated from CD experiments.[28]

However, the presence of the trehalose environment appears to preserve the structural content of the protein solution. Our efforts in using trehalose to prevent this nanoparticle induced denaturation and subsequent aggregation of protein are based on the underlying hypothesis that the trehalose molecules stabilize the natively folded structure of protein, which binds electrostatically to the negatively charged nanoparticle surface through the positively charged surface domains. Through the
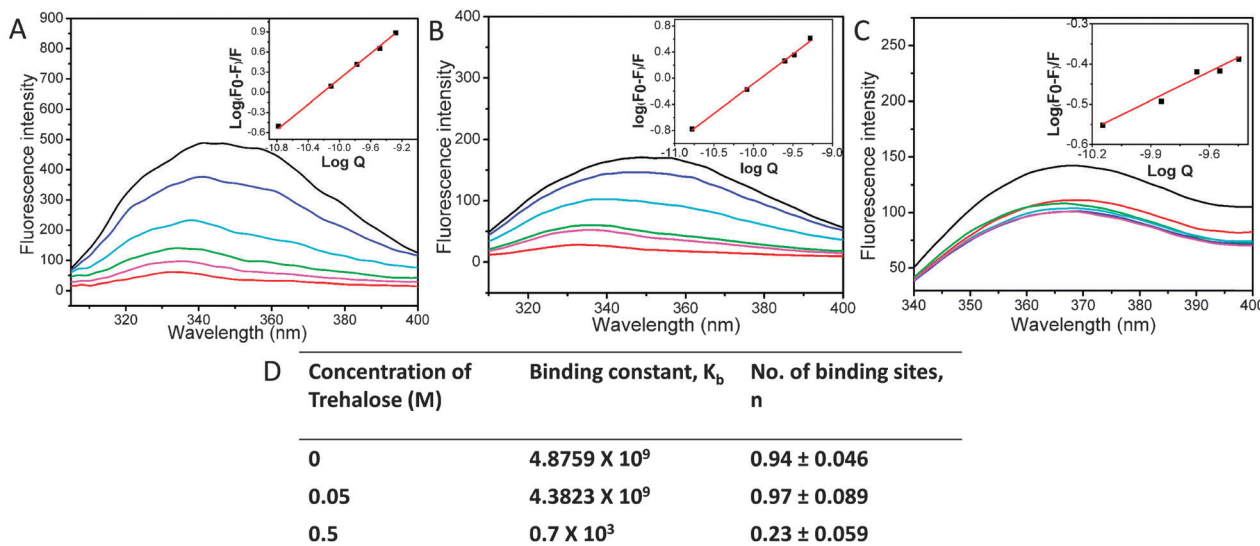
Fig. 3 (A), (B) and (C) shows tryptophan fluorescence quenching in the presence of different concentrations of Ag nanoparticles in 0, 0.05 and 0.5 M trehalose solution respectively. The black, blue, cyan, green, red and orange curves corresponds to nanoparticle concentrations of 0.005, 0.167, 0.0167, 0.083, 0.33 and 0.5 nM respectively. The insets show the plot of log $(F_0 - F)/F$ as a function of log Q. (D) Shows the binding constants and no. of binding sites of lysozyme at different concentrations of trehalose.

Concentration of Trehalose (M)	Binding constant, K_b	No. of binding sites, n
0	4.8759×10^9	0.94 ± 0.046
0.05	4.3823×10^9	0.97 ± 0.089
0.5	0.7×10^3	0.23 ± 0.059

enhanced hydrogen bonding with the protein side-chains and the sequestration effect of the trehalose molecules, we expect that the direct and structure altering interaction between the protein and nanoparticles can be minimized, thus retaining the secondary structure of the native protein. This behaviour is confirmed by the CD experiments on the nanoparticle–protein conjugates in the presence of trehalose. Even an intermediate trehalose concentration of 0.05 M was found to be sufficient to maintain the α-helix content (24.40%) (blue curve) almost similar to that of lysozyme in phosphate buffer (23.45%). Furthermore, the α-helix content was found to be 33.01% in the presence of 0.5 M trehalose (green curve). This is similar to the α-helix content (33%) computed in the absence of nanoparticles in 0.5 M trehalose (cyan curve). Importantly, as anticipated, the helicity of proteins is conserved by the presence of trehalose similar to glycerol and other polyols.[29,30] Our results on trehalose, therefore, reiterate its structure preserving properties.

Fluorescence quenching studies of the lysozyme–nanoparticle conjugates

To further substantiate the nature of lysozyme–nanoparticle interactions, we performed fluorescence quenching studies. Clearly, in the presence of nanoparticles, concentration dependent fluorescence quenching of lysozyme can be seen (Fig. 3). This phenomenon is also known as nano-material surface energy transfer,[31] where energy transfer occurs between the molecular dipole of the chromophore and the nanoparticle surface leading to quenching. The quenching also suggests the attachment and probable denaturation of protein upon interaction with the surface.[32] Lysozyme consists of 6 tryptophan residues, which are proximal to its substrate binding site at positions 28, 62, 63, 108, 111 and 123. These residues act as the most dominant fluorophores for the study of fluorescence quenching. The binding

modes and the number of binding sites can be calculated by the following equation:[33]

$$\log \frac{F_0 - F}{F} = \log k_b + n \log Q$$

where F_0 and F are the fluorescence intensities in the absence and presence of the quencher respectively. The plot of log k_b *vs.* log Q gives the value of binding constant k_b and no. of binding sites n. The values of k_b and n are tabulated in Fig. 3D for three different concentrations of trehalose, namely 0 M, 0.05 M and 0.5 M respectively.

The value of k_b for the lysozyme–nanoparticle system in the 0.05 M trehalose solution exhibits a slight decrease in relation to that in the absence of trehalose. In the case of 0.5 M trehalose solution, the binding constant is greatly reduced. This indicates that a concentration of 0.5 M trehalose affects the binding of the protein to the silver nanoparticles to a large extent. The value of n is also much lesser for 0.5 M trehalose solution, which leads to the conclusion that lysozyme at a trehalose concentration of 0.5 M trehalose solution cannot efficiently interact with the surface of the silver nanoparticles. On the other hand, the concentration of 0.05 M trehalose does not appear to effectively prevent the interaction of lysozyme and silver nanoparticles. The values of n in the absence of trehalose and in the presence of 0.05 M trehalose are nearly 1. A value of $n < 1$ observed in the case of the presence of 0.5 M trehalose indicates the decrease of the overall binding strength of the protein to the surface of the nanoparticles.[34] These results also highlight the role of trehalose in the modulation of surface attachment of the protein molecules to the surface of the nanoparticles.

UV-vis absorbance studies on lysozyme–nanoparticle conjugates

UV-vis absorbance spectroscopy is used to characterize the optical properties of the silver nanoparticles. Additionally, the
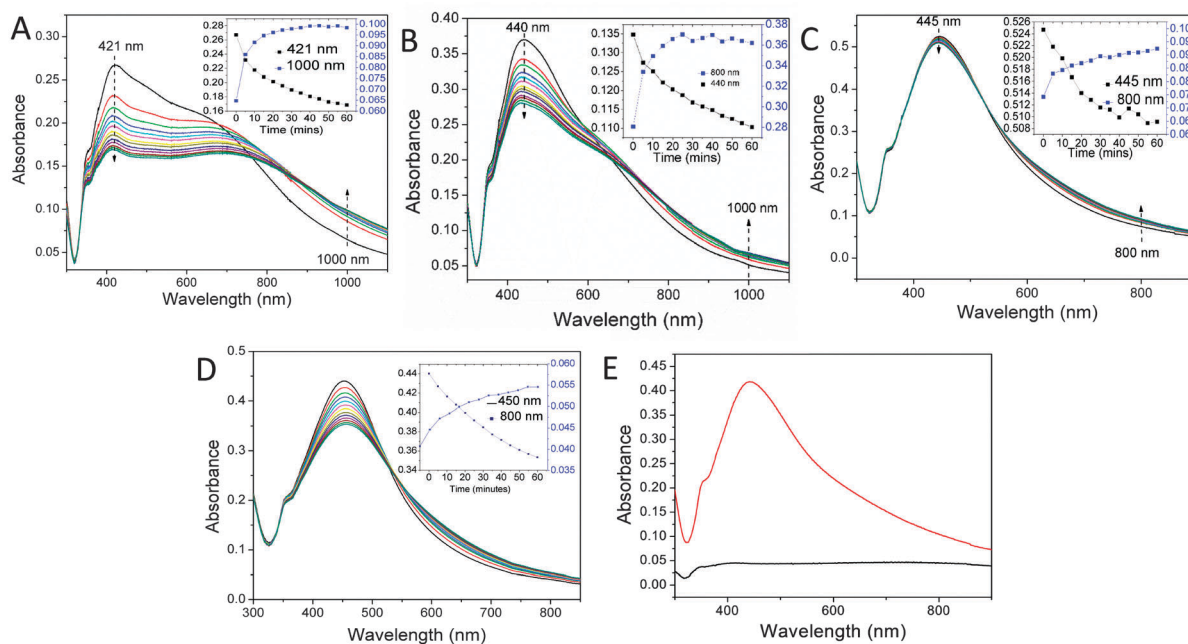
Fig. 4 (A–C) UV-vis spectra showing aggregation behaviour of Ag nanoparticles in the presence of lysozyme with trehalose concentrations 0, 0.05 M and 0.5 M respectively. (D) UV-vis spectra of lysozyme–nanoparticle conjugates in the presence of 1 M sucrose. The insets (A–D) show the evolution of the transverse (black) and longitudinal (blue) plasmon mode with time. (E) UV-vis spectra of lysozyme–nanoparticle conjugate (black) and lysozyme–nanoparticle conjugate in the presence of 0.5 M trehalose concentration after 24 hours (red).

size, shape and the nature of dispersion can be estimated from the surface plasmon resonance band. For smaller nanoparticles, the surface plasmon resonance consists of a single dipolar mode. The shape and the coupling of nanoparticles in the form of aggregation greatly affect the surface plasmon resonance of the nanoparticles. The anisotropy introduced in the structure through aggregation induced coupling or by non-spherical structures gives rise to absorption at lower energies creating higher order multi-polar modes.[35] The nanoparticles exhibited a surface plasmon resonance mode at 420 nm. Trehalose induces a change in the dielectric constant around the nanoparticle which shifts the peak to a higher wavelength at around 450 nm. In the presence of lysozyme, the dipolar (transverse) plasmonic mode of the Ag nanoparticle (between 420–450 nm) decreased in intensity with time, whereas the intensity of the longitudinal mode showed a corresponding rise (Fig. 4A). This indicates the typical aggregation behaviour of the protein–nanoparticle system where the proteins that are attached to the nanoparticles form aggregates, thus inducing (secondary) aggregate formation among the nanoparticles themselves.[16] This aggregation can be observed for a wide range of protein concentrations (Fig. S1, ESI†) thus ruling out aggregation behaviour observed in the presence of salts (Fig. S2, ESI†), where both the dipolar and longitudinal modes exhibit a temporal decrease in intensity.[36]

Similarly, the presence of trehalose in protein–nanoparticle solution presents markedly lesser changes in the intensities of the dipolar and longitudinal plasmon modes and exhibits a clear trend when the trehalose concentration is increased from 0 M to 0.05 M and 0.5 M (Fig. 4A–C). As the concentration of trehalose was increased to 0.05 M and 0.5 M, the previously seen variations

in the case of 0 M trehalose (Fig. 4A) in both the dipolar and longitudinal plasmon modes in opposite directions were largely suppressed – hinting at the decrease in clustering of nanoparticles. Two possible explanations can be put forth for the observation of this behaviour. First, as seen from the fluorescence measurements, the reduction in the binding of proteins to the silver nanoparticles decreases the formation of seeds for the aggregation of proteins. Second, the free proteins in the trehalose-containing solution have a reduced tendency to form protein aggregates on the surface of the silver nanoparticles. Importantly, the UV-vis spectrum obtained – even after 24 hours of incubation of the protein–nanoparticle solution – shows the presence of the dipolar plasmon mode (Fig. 4E). In contrast, in the case of the protein–nanoparticle solution without trehalose, there is almost complete reduction of the dipolar plasmon mode due to substantial aggregation of the protein–nanoparticle conjugate. Interestingly, even a 1 M sucrose solution (*i.e.* twice the maximum concentration of trehalose used here) showed a substantial decrease in the dipolar plasmonic mode in relation to the protein–nanoparticle conjugate observed in the presence of trehalose (Fig. 4D). Evidently, the presence of a higher concentration of sucrose does not prevent the aggregation of the protein–nanoparticle conjugate. Taken together, these results highlight the remarkable efficacy of trehalose in the prevention of protein–nanoparticle aggregation – even in comparison to similar carbohydrates.

Imaging of the lysozyme–nanoparticle conjugates

The aggregate formation observed clearly through UV-vis spectroscopy was imaged through confocal fluorescence microscopy.
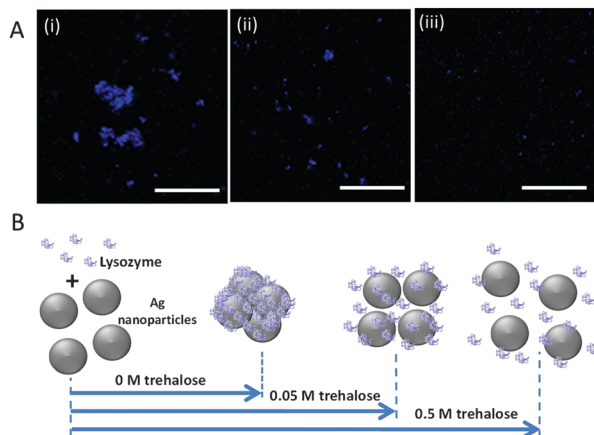
Fig. 5 (A) (i–iii) False color fluorescence images arising from lysozyme aggregated silver nanoparticles in the presence of 0, 0.05 and 0.5 M trehalose solution respectively (scale bar represents 10 μm); and (B) schematic showing the likely effect of trehalose on protein–nanoparticle aggregation.

Fig. 6 SERS spectrum of (A) lysozyme–nanoparticle conjugate, (B) lysozyme–nanoparticle conjugate in the presence of 0.05 M trehalose, (C) lysozyme–nanoparticle conjugate in the presence of 0.5 M trehalose, (D) Ag nanoparticles in 0.5 M trehalose and (E) Ag nanoparticles in PBS buffer. Inset: (i–v) shows the 242 cm^{-1} mode for spectra A–E.

It is known that silver nanoparticles cluster in biological medium and the plasmon resonance resulting due to incident laser radiation gives rise to far red fluorescence.[37] This can help in tracking metal nanoparticles even inside cells.[37] Likewise, in the presence of lysozyme, the silver nanoparticle clusters exhibit far-red fluorescence. Fig. 5A displays false-color far red fluorescence images that correlate with the sizes and extent of aggregation of the nanoparticles occurring in the presence of lysozyme and different concentrations of trehalose. It can be clearly seen that in the absence of trehalose, the size of the silver nanoparticle aggregates are much bigger than in the presence of trehalose. In the presence of 0.05 M trehalose, the aggregates are much smaller and at 0.5 M trehalose the fluorescence becomes almost non-discernible through the naked eye. The imaging and aggregation experiments can be summarized in the form of a schematic which is shown in Fig. 5B. The schematic shows the formation of different degrees of aggregation of nanoparticles in the presence of lysozyme and different concentrations of trehalose. The representation conveys the fact that the increase in trehalose concentration stabilizes the protein structure and also reduces the binding of lysozyme molecules to the surface of the nanoparticles thus preventing the aggregation of the protein–nanoparticle conjugate.

SERS studies on lysozyme–nanopaticle interactions

In order to further investigate the specific structural aspects at more localized portions of protein molecules, the highly surface-selective technique SERS was employed. Due to this surface-selectivity, SERS has been exploited, by us and others, for protein based studies[37–40] and to detect minute structural changes in the adsorption of proteins to the nanoparticle surface.[41] Here, SERS spectra with high signal-to-noise ratio were recorded from lysozyme–nanoparticle conjugates in the presence of 0 M and 0.05 M trehalose (Fig. 6A and B); however, the modes of lysozyme in 0.5 M trehalose were not strongly enhanced (Fig. 6C). This can be attributed to the decrease in interaction between the protein and nanoparticle surface, which was independently corroborated
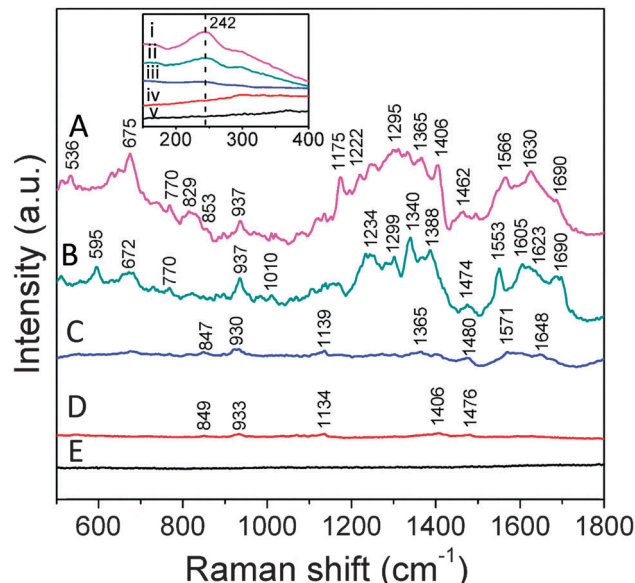
by fluorescence quenching experiments. In the case of 0.5 M trehalose, the binding constant was significantly reduced, which was not observed for the 0.05 M trehalose concentration.

Analysis of SERS spectra

The SERS spectrum of lysozyme is dominated by vibrational modes of aromatic amino acids Phe, Tyr, Trp and His as well as amide and backbone spectral features (Fig. 6) and is consistent with the existing literature.[40,42,43] It is worth mentioning that the appearance and the intensity of the modes of the protein are governed by its orientation to the surface of the nanoparticles taking into account the surface selection rules.[44] Since the electromagnetic field enhancement decays as the third power of the radial distance from the surface, the vibrational modes lying close to the surface undergoes preferential enhancement than those lying afar.[45]

Notably, the SERS spectrum of lysozyme–nanoparticle conjugate in 0.05 M trehalose solution displayed key differences in relation to the spectrum acquired in the absence of trehalose. The detailed band assignments are provided in Table 1. We have also recorded the SERS spectra of the nanoparticles in buffer (PBS) (Fig. 6E) as well as the SERS (Fig. 6D) from Ag nanoparticles in trehalose solution (0.5 M). These spectral profiles were recorded to ascertain that they do not contribute to the SERS spectra of lysozyme. In the ensuing paragraphs, we discuss the important modes arising from different groups of lysozyme and how they are affected by the presence of trehalose.

Aromatic amino acids

The spectra of lysozyme are dominated by peaks from aromatic amino acids. Modes corresponding to Phe are found at 1175, 1474, and 1605 cm^{-1}. They correspond to the modes ν_{9a}, ν_{19b}

Table 1 SERS band assignments for lysozyme.[39,40,42,43,46–50] The modes present in the spectrum of lysozyme alone in the absence of trehalose are marked with *

Peak (cm^{-1})	Proposed band assignments and residues
242*	Ag–N
536*	ν(S–S)
595	Trp
672, 675*	Tyr, ν(C–S)
770*	Trp (W$_{19}$) or His
829*	Tyr
847, 853*	Tyr
930, 937*	ν(C–COO$^-$)/α-helical C–C stretching vibration
1010	Trp(W$_{16}$)
1139	ν_{as}(C$_\alpha$CN)
1175*	Tyr or Phe(ν_{9a})
1222*	Amide III
1234	Amide III/Trp
1295*/1299	Amide III
1340	Trp$_{W7}$ and/or δ(CH)
1365*	Trp$_{W7}$ and/or δ(CH)
1388	ν(COO$^-$)
1406*	ν_s(COO$^-$)
1462	δ(CH$_2$)/δ(CH)
1474	δ(CH$_2$)/δ(CH), N–H deformation, Trp, His, Phe, Tyr
1553	Trp, His and/or Amide II
1566*	ν_{as}(COO$^-$), His, Trp$_{W2}$
1605	Trp$_{W1}$, Tyr, and/or Phe(ν_{8a})
1623, 1630*, 1648	Amide I
1690*	Amide I

and phenyl C stretching ν_{8a} respectively.[42,46] The region from 1300 to 1500 cm^{-1} also contains δ(CH$_2$) modes from phenylalanine. Modes from the tyrosine residues also occur at 675, 829, 853 and 1175 cm^{-1}. The characteristic tyrosine doublet arising from the Fermi resonance between the ring breathing mode and the overtone of out-of-plane ring bending vibrations of the *para*-substituted benzenes can be found at 829 and 853 cm^{-1} respectively.[47]

Aliphatic side chain vibrations

The carboxy group stretching vibrations C–COO$^-$ occur at 930, 1388, 1406 and 1566 cm^{-1}. These are the constituents of the side groups of acidic amino acids glutamic acid and aspartic acid.[39] There are several overlaps of asymmetric stretching vibrations of the COO$^-$ group at around 1550 cm^{-1} with His, Trp and Phe bands. The CH$_2$ wagging and deformation modes can be found at around 1360 and 1470 cm^{-1}, respectively. The C–N stretching mode and C–NH$_2$ group vibrations can be found at 1139 cm^{-1} and in the 1050–1200 cm^{-1} region, respectively. The mode at 1340 cm^{-1} can be assigned to modes corresponding to C$_\alpha$–H bending and C–C$_\alpha$ stretching.

Amide vibrations

The modes most sensitive to the secondary structure of protein are the amide I modes. They consist of a combination of CO stretching vibrations with contributions from N–H bending as well as C–N stretching vibrations.[48] Amide II is a Raman inactive mode but becomes active in the case of SERS due to the modification of the surface selection rules. It consists of a combination of NH in-plane bending and CN stretching vibrations as well as CO in-plane bending and CC and NC stretching

vibrations. The amide III mode arises due to NH bending and CN stretching vibrations with contributions from CO in-plane bending and CC stretching vibrations. Specifically, the amide I peak resides in the range of 1600–1750 cm^{-1}. Amide II and amide III are found at around 1553 and 1222/1234 cm^{-1} respectively.[48] In the case of lysozyme, the modes at 1630 (shifted to 1648 cm^{-1} in the presence of 0.5 M trehalose) and 1690 cm^{-1} can be assigned to amide I for α-helix and random coils, respectively. These can be directly correlated with the structure of lysozyme, which consists of a well-defined α-helical domain and an antiparallel β-sheet domain that are joined by random coils. In the presence of 0.05 M trehalose, we also observe a feature at 1623 cm^{-1}, which may be ascribed to the presence of antiparallel β-sheets.[48]

The disulphide and the Ag–N bonds

The lysozyme molecule contains two pairs of disulphide bonds in α-helical and β-sheet domains. The corresponding modes can be seen at around 536 cm^{-1}. In addition, the mode at 242 cm^{-1} can be assigned to the Ag–N stretching vibration.[49]

Effect of trehalose on SERS spectra of lysozyme

Significant spectral changes of lysozyme take place at different concentrations of the trehalose environment. The most important changes which occur in the SERS spectra due to the presence of trehalose are: (A) the change in binding of the lysozyme molecules to the surface of the nanoparticles and (B) the alteration in the lysozyme structure and orientation with respect to the surface of the nanoparticles. Visual inspection reveals that the SERS intensity of the lysozyme–nanoparticle conjugate is quite pronounced in the absence of trehalose as well as in the presence of 0.05 M trehalose in the medium. The significantly lower SERS intensity of lysozyme in the presence of 0.5 M trehalose hints at the reduced attachment of the lysozyme molecules to the surface of the nanoparticles (as also revealed by the fluorescence quenching studies).

The mode at 242 cm^{-1} corresponding to the Ag–N stretching mode also indicates direct chemical interaction of the lysozyme with the surface of the metal nanoparticles. In the absence of trehalose, this mode is the strongest followed by the cases of 0.05 M and 0.5 M trehalose in sequence. In the case of spectra recorded from the nanoparticles in buffer or trehalose solution, this mode is negligible in intensity, which indicates that trehalose itself does not form chemical bond(s) with the surface of the nanoparticles.

The changes in structural aspects of the proteins can be deciphered from the significant differences of the modes related to Tyr and Trp, and the amide features. It is known that the orientation of the rings of the aromatic amino acids to the surface of the nanoparticles affects the SERS spectra. The modes corresponding to A$_1$ and A$_g$ have polarizability components in all three axes, whereas the B$_1$ and B$_{2g}$ modes have polarizability components in particular directions. Therefore, these modes behave differentially with respect to their orientation to the metal surface.[46,50] The changes of modes at 595, 829, 853, 1010, 1175, 1234, 1553 and 1566 cm^{-1} between the spectra

of lysozyme in the presence of 0 and 0.05 M trehalose mostly correspond to the peaks arising from the aromatic amino acids. As detailed above, the amide features, and particularly the amide I region, provide important clues to the structure of the lysozyme under different conditions. In general, we also see the broadening of the modes in the case of SERS of lysozyme in the absence of trehalose, which is an indication of aggregation behaviour of the protein in the presence of the nanoparticles.[43] Taken together, the changes in the presence/intensity of various modes provide compelling evidence of alterations in protein structure and aggregation behaviour in the presence of nanoparticles and critically highlight the stabilizing influence of trehalose.

Conclusions

While nanoparticles represent a rapidly emerging instrument in the biomedical tool kit, clinical translation of their theranostic potential is incomplete. A critical impediment in the more comprehensive application of nanoparticle platforms is the adverse side effects experienced by a biological system – as illustrated by the disruptive changes induced in protein structures. For instance, nanoparticles have been known to disrupt protein systems by inducing fibril formation.[51] Here, we have been able to create a condition in which the nanoparticles and the protein co-exist together without having any adverse effect on the protein structure. This is of vital importance in enabling analytical measurements that require tailored nanoparticle protein complexes. SERS applications on proteins have been very limited since it requires direct contact with the nanoparticle surface with the retention of their functions. Our results, however, provide strong evidence that using optimal concentrations of osmolytes like trehalose, the protein–nanoparticle interaction can be modulated and the protein can actually interact with the nanoparticle surface without undergoing major structural changes. We envision that this approach will play an important role in the formulation of combined multi-therapeutics and in theranostic nanomedicine where designed nanoplexes are sought to glean diagnostic insight for well-informed, personalized treatment.

Notes and references

1 R. Singh and J. W. Lillard Jr, *Exp. Mol. Pathol.*, 2009, **86**, 215–223.

2 R. A. Petros and J. M. DeSimone, *Nat. Rev. Drug Discovery*, 2010, **9**, 615–627.

3 J. Shang and X. Gao, *Cell Biosci.*, 2014, **4**, 1–2.

4 P. V. AshaRani, G. Low Kah Mun, M. P. Hande and S. Valiyaveettil, *ACS Nano*, 2009, **3**, 279–290.

5 M. N. Moore, *Environ. Int.*, 2006, **32**, 967–976.

6 B. Leader, Q. J. Baca and D. E. Golan, *Nat. Rev. Drug Discovery*, 2008, **7**, 21–39.

7 M.-E. Aubin-Tam, in *Nanomaterial Interfaces in Biology*, ed. P. Bergese and K. Hamad-Schifferli, Humana Press, 2013, vol. 1025, ch. 3, pp. 19–27.

8 N. Casadevall, J. Nataf, B. Viron, A. Kolta, J.-J. Kiladjian, P. Martin-Dupont, P. Michaud, T. Papo, V. Ugo, I. Teyssandier, B. Varet and P. Mayeux, *N. Engl. J. Med.*, 2002, **346**, 469–475.

9 G. R. Zimmermann, J. Lehár and C. T. Keith, *Drug Discovery Today*, 2007, **12**, 34–42.

10 T. Arakawa and S. N. Timasheff, *Biochemistry*, 1982, **21**, 6536–6544.

11 U. Jakob, M. Gaestel, K. Engel and J. Buchner, *J. Biol. Chem.*, 1993, **268**, 1517–1520.

12 J. K. Kaushik and R. Bhat, *J. Biol. Chem.*, 2003, **278**, 26458–26465.

13 N. K. Jain and I. Roy, *Current Protocols in Protein Science*, John Wiley & Sons, Inc., 2001.

14 M. Sola-Penna and J. R. Meyer-Fernandes, *Arch. Biochem. Biophys.*, 1998, **360**, 10–14.

15 A. Eroglu, M. J. Russo, R. Bieganski, A. Fowler, S. Cheley, H. Bayley and M. Toner, *Nat. Biotechnol.*, 2000, **18**, 163–167.

16 D. Zhang, O. Neumann, H. Wang, V. M. Yuwono, A. Barhoumi, M. Perham, J. D. Hartgerink, P. Wittung-Stafshede and N. J. Halas, *Nano Lett.*, 2009, **9**, 666–671.

17 P. C. Lee and D. Meisel, *J. Phys. Chem.*, 1982, **86**, 3391–3395.

18 J. Yguerabide and E. E. Yguerabide, *Anal. Biochem.*, 1998, **262**, 137–156.

19 C. D. Keating, K. M. Kovaleski and M. J. Natan, *J. Phys. Chem. B*, 1998, **102**, 9404–9413.

20 G. Brancolini, D. B. Kokh, L. Calzolai, R. C. Wade and S. Corni, *ACS Nano*, 2012, **6**, 9863–9878.

21 V. Lechevalier, T. Croguennec, S. Pezennec, C. Guérin-Dubiard, M. Pasco and F. Nau, *J. Agric. Food Chem.*, 2003, **51**, 6354–6361.

22 K. GEKKO, *J. Biochem.*, 1982, **91**, 1197–1204.

23 L. Calzolai, F. Franchini, D. Gilliland and F. Rossi, *Nano Lett.*, 2010, **10**, 3101–3105.

24 N. J. Greenfield, *Nat. Protoc.*, 2007, **1**, 2876–2890.

25 N. Sreerama, S. Y. Venyaminov and R. W. Woody, *Anal. Biochem.*, 2000, **287**, 243–251.

26 N. J. Greenfield and G. D. Fasman, *Biochemistry*, 1969, **8**, 4108–4116.

27 A. Sethuraman and G. Belfort, *Biophys. J.*, 2005, **88**, 1322–1333.

28 S. Q. Luo, C. Y. F. Huang, J. F. McClelland and D. J. Graves, *Anal. Biochem.*, 1994, **216**, 67–76.

29 T. Knubovets, J. J. Osterhout, P. J. Connolly and A. M. Klibanov, *Proc. Natl. Acad. Sci. U. S. A.*, 1999, **96**, 1262–1267.

30 K. Fu, K. Griebenow, L. Hsieh, A. M. Klibanov and L. Robert, *J. Controlled Release*, 1999, **58**, 357–366.

31 S. H. D. P. Lacerda, J. J. Park, C. Meuse, D. Pristinski, M. L. Becker, A. Karim and J. F. Douglas, *ACS Nano*, 2010, **4**, 365–379.

32 L. Shang, Y. Wang, J. Jiang and S. Dong, *Langmuir*, 2007, **23**, 2714–2721.

33 A. Chaudhary, A. Gupta, S. Khan and C. K. Nandi, *Phys. Chem. Chem. Phys.*, 2014, **16**, 20471–20482.

34 S. P. Boulos, T. A. Davis, J. A. Yang, S. E. Lohse, A. M. Alkilany, L. A. Holland and C. J. Murphy, *Langmuir*, 2013, **29**, 14984–14996.

35 S. Link and M. A. El-Sayed, *Int. Rev. Phys. Chem.*, 2000, **19**, 409–453.

36 L. Stebounova, E. Guio and V. Grassian, *J. Nanopart. Res.*, 2011, **13**, 233–244.

37 K. Kneipp, H. Kneipp, I. Itzkan, R. R. Dasari and M. S. Feld, *J. Phys.: Condens. Matter*, 2002, **14**, R598–R694.

38 Z. Zhou, X. Han, G. G. Huang and Y. Ozaki, *J. Raman Spectrosc.*, 2012, **43**, 706–711.

39 S. Siddhanta, D. Karthigeyan, P. P. Kundu, T. K. Kundu and C. Narayana, *RSC Adv.*, 2013, **3**, 4221–4230.

40 E. López-Tobar, B. Hernández, J. Gómez, A. Chenal, J. V. Garcia-Ramos, M. Ghomi and S. Sanchez-Cortes, *J. Phys. Chem. C*, 2015, **119**, 8273–8279.

41 D. Karthigeyan, S. Siddhanta, A. H. Kishore, S. S. R. R. Perumal, H. Ågren, S. Sudevan, A. V. Bhat, K. Balasubramanyam, R. K. Subbegowda, T. K. Kundu and C. Narayana, *Proc. Natl. Acad. Sci. U. S. A.*, 2014, **111**, 10416–10421.

42 J. Hu, R. S. Sheng, Z. S. Xu and Y. e. Zeng, *Spectrochim. Acta, Part A*, 1995, **51**, 1087–1096.

43 G. Chandra, K. S. Ghosh, S. Dasgupta and A. Roy, *Int. J. Biol. Macromol.*, 2010, **47**, 361–365.

44 S. Schlücker, *Angew. Chem., Int. Ed.*, 2014, **53**, 4756–4795.

45 S. Siddhanta and C. Narayana, *Nanomater. Nanotechnol.*, 2012, **2**, 1–13.

46 C. Gullekson, L. Lucas, K. Hewitt and L. Kreplak, *Biophys. J.*, 2011, **100**, 1837–1845.

47 M. N. Siamwiza, R. C. Lord, M. C. Chen, T. Takamatsu, I. Harada, H. Matsuura and T. Shimanouchi, *Biochemistry*, 1975, **14**, 4870–4876.

48 A. Barth and C. Zscherp, *Q. Rev. Biophys.*, 2002, **35**, 369–430.

49 M. Bolboaca, W. Kiefer and J. Popp, *J. Raman Spectrosc.*, 2002, **33**, 207–212.

50 F. R. Dollish, W. G. Fatalev and F. F. Bentley, *Characteristic Raman Frequencies of Organic compounds*, Wiley, New York, 1974.

51 S. C. Wagner, M. Roskamp, M. Pallerla, R. R. Araghi, S. Schlecht and B. Koksch, *Small*, 2010, **6**, 1321–1328.